

Electron-phonon couplings in locally disordered materials: The case of hybrid halide perovskites

Marios Zacharias,^{1,*} George Volonakis,² Laurent Pedesseau,¹
Claudine Katan,² Feliciano Giustino,^{3,4} and Jacky Even^{1,†}

¹*Univ Rennes, INSA Rennes, CNRS, Institut FOTON - UMR 6082, F-35000 Rennes, France*

²*Univ Rennes, ENSCR, INSA Rennes, CNRS, ISCR - UMR 6226, F-35000 Rennes, France*

³*Oden Institute for Computational Engineering and Sciences,*

The University of Texas at Austin, Austin, Texas 78712, USA

⁴*Department of Physics, The University of Texas at Austin, Austin, Texas 78712, USA*

(Dated: June 16, 2025)

Positional polymorphism in solids refers to distributions of correlated locally disordered unit cells which reflect, on average, the high-symmetry structure observed in diffraction experiments. The standard theory of electron-phonon interactions is unable to account for the temperature-dependent electronic structure of polymorphous materials. A prime example of such materials is hybrid halide perovskites, for which calculations of band gaps at finite temperatures do not agree with experiment. Here, we develop a systematic and accurate methodology to investigate electron-phonon couplings in complex polymorphous materials, demonstrated through calculations of anharmonic phonons and thermally-induced band gap renormalization for a broad family of halide perovskites. Our approach delivers unprecedented agreement with experiment.

Recently, the concept of correlated local disorder (positional polymorphism) has gained significant attention across a broad range of materials^{1–9}. In perovskites, local disorder has been observed experimentally since the 1960s¹⁰, and later confirmed through X-ray and neutron scattering as well as nuclear magnetic resonance measurements^{7,8,11–25}. A prominent class of such materials is hybrid halide perovskites^{1,12}, which exhibit high efficiency and favorable optoelectronic properties, making them excellent candidates for energy applications such as photovoltaics and light-emitting devices^{26–32}. To realize the full potential of halide perovskites, a fundamental understanding of positional polymorphism and its interplay with the electronic, vibrational, and electron-phonon properties is essential.

Hybrid ABX_3 halide perovskites are composed of an organic molecule (A) and an inorganic network formed by metal cations (B) octahedrally coordinated by halide anions (X) [Figs. 1(a,b)]. One central assumption in static density functional theory (DFT) calculations for tetragonal or cubic hybrid halide perovskites is the use of a periodic high-symmetry (monomorphous) metal-halide network^{32–40}. The orientation of the molecule A is typically randomly chosen or set to towards an unrealistic static direction. Critical issues related to the use of a high-symmetry inorganic network include (i) neglecting important corrections to the electronic structure¹, (ii) the breakdown of the standard harmonic approximation to describe lattice dynamics⁴¹, (iii) neglecting energetically more stable configurations and thus overlooking important structural features impacting chemical bonding and optoelectronic properties^{42–44}, and (iv) ignoring important modifications to electron-phonon coupling (EPC)⁶.

An approach for more accurate static DFT calculations using locally disordered (polymorphous) perovskites has been proposed^{1,4}. It has been shown that accounting for symmetry-breaking domains in tetragonal and cubic

perovskites yields considerably improved agreement with measurements on pair distribution functions, band gaps, and effective masses^{1,4,6}. Although molecular dynamics simulations^{22,24,52–60} can capture local disorder through long equilibration times, a direct distinction between local disorder and thermal vibrations is inevitably missed.

Recently, we have introduced a bottom-up first-principles approach⁶, showing that local disorder in *inorganic* halide perovskites ($A=Cs$) yields dynamically stable and strongly interacting phonons, and affects profoundly anharmonic EPCs. This polymorphous framework can be seen as a quasi-static approximation of the slow relaxation dynamics of the structure. In this Letter, we explore the more challenging and technologically relevant cases of hybrid halide perovskites and compare with their inorganic counterparts. Together with Ref. [45], we propose an efficient approach to evaluate phonons and temperature-dependent band gaps of polymorphous cubic $APbBr_3$, $APbI_3$, and $ASnI_3$, where A = methylammonium (MA) or formamidinium (FA). Our calculations agree with experiments for all cases, as shown in Fig. 1, opening the way for high-throughput, efficient, and accurate predictions of anharmonic electron-phonon properties of complex polymorphous systems.

DFT calculations were performed using **Quantum Espresso**^{61,62} in conjunction with optimized norm-conserving Vanderbilt pseudopotentials^{63,64} and the Perdew-Burke-Ernzerhof exchange-correlation functional revised for solids (PBEsol)⁶⁵; full computational details are available in Ref. [45]. In Figs. 1(a)-(f), we show the geometries of the cubic $FAPbI_3$ and $ASnI_3$. We consider three cases: (i) the monomorphous structure represented by a minimal unit cell [i.e. the formula unit (f.u.)] where the atoms of the inorganic network reside at their high-symmetry positions and the FA or MA molecules point towards a single orientation [Figs. 1(a) and (b)], (ii) the reference structure represented by a supercell where

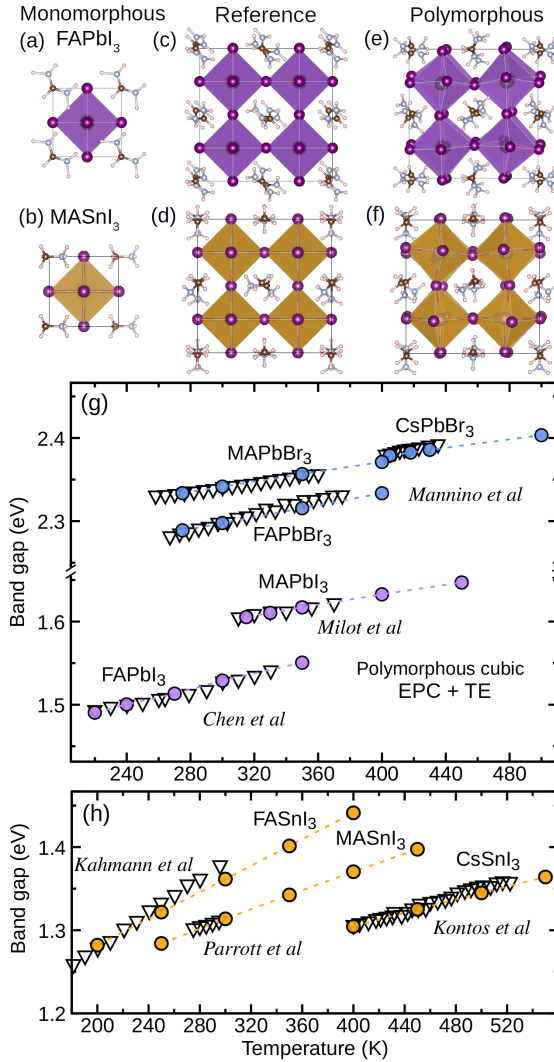


FIG. 1. (a-f) Ball and stick models of cubic FAPbI₃ and MASnI₃ representing monomorphous (a,b), reference (c,d), and polymorphous (e,f) structures. Structures in (a,b) refer to unit cells (12 atoms), in (c,d,e,f) to 2×2×2 supercells. (g,h) Calculated temperature-dependent band gaps (coloured discs) of Pb (g) and Sn (h) cubic hybrid halide perovskites including electron-phonon coupling (EPC) and thermal expansion (TE) effects; EPC is incorporated via the ASDM using ZG polymorphous structures and TE contribution is evaluated by allowing lattice expansion according to the experimental expansion coefficients⁴⁵. Experimental gaps (triangles) are from Refs. [46–51]. ASDM calculations refer to 4×4×4 supercells (768 atoms) and the DFT-PBEsol including spin orbit coupling (SOC). The data are shifted close to PBE0 corrections reported in Ref. [45] to match experiment.

the atoms of the inorganic network are fixed at their high-symmetry positions and the FA or MA molecules are relaxed starting from random orientations [Figs. 1(c) and (d)], (iii) the polymorphous structure represented by a supercell where the atoms of the inorganic network and

FA or MA molecules are relaxed starting from the reference structure [Figs. 1(e) and (f)]. During relaxations, the lattice constants are fixed at their experimental values⁴⁵. We consider reference configurations since changes in the electronic structure and phonons are sensitive to the net dipole moments induced by the single cation orientation in the monomorphous structure and to ensure a consistent comparison with the results for the polymorphous structures. In Cs-based compounds, the reference is identical to the monomorphous structure so no special treatment is required. Additionally, to assess the electronic structure and thermal effects variability of the polymorphous networks originating from various molecular orientations^{52,66}, we generate 10 distinct polymorphous structures and take averages⁴⁵.

To compute thermal band gap renormalization, we consider both EPC and lattice thermal expansion (TE) so that the band gap temperature coefficient is given by⁶⁷:

$$dE_g/dT = dE_g/dT|_{\text{EPC}} + dE_g/dT|_{\text{TE}}. \quad (1)$$

We use temperature-dependent phonons computed within the self-consistent phonon theory as implemented in the anharmonic special displacement method⁴¹ (ASDM). This requires computing interatomic force constants iteratively of the corresponding thermally displaced reference structures until convergence in the phonons and system's free energy⁴⁵. The computed dynamically stable phonons allow us to include phonon anharmonicity in nonperturbative calculations of EPC via the special displacement method^{6,68,69}. That is we apply special Zacharias-Giustino (ZG) displacements⁴⁵ starting from the polymorphous structures. To account for TE, we expand the lattice based on the experimental expansion coefficients^{47,70–81}, as described in Ref. [45].

In Figs. 1(g,h), we compare our calculations for temperature-dependent band gaps of polymorphous cubic MAPbBr₃, MAPbI₃, FAPbBr₃, FAPbI₃, FASnI₃, and MASnI₃ with experiments^{46–51}. We include data for CsPbBr₃ and CsSnI₃ for completeness⁴⁵. Calculations and experiments agree for all compounds, showcasing the broad applicability of our approach in describing anharmonic electron-phonon renormalized band structures. Quantitative agreement is further evidenced by our calculated dE_g/dT reported in Table I, in which we further provide data for CsPbI₃⁴⁵. We also show the EPC contribution to the gap renormalization for all materials, varying between 27–97%. For the majority of compounds, EPC plays a dominant role in band gap renormalization, challenging the prevailing view that TE and EPC contribute equally in lead halide perovskites^{82,83}. A clear trend is observed in the variation of the EPC contribution across all compounds, with its percentage increasing as the A-site cation changes from FA to MA and then to Cs. For example, in FAPbBr₃ and FASnI₃, EPC contributes only 27% and 34%, respectively. This relatively lower contribution is not surprising, as their volumetric TE coefficients are among the highest reported for halide perovskites⁷⁷. Sn-based compounds exhibit a

TABLE I. Band gap temperature coefficient (dE_g/dT) of cubic halide perovskites. r- and p- stand for reference and polymorphous. Experimental values are extracted by linear fits⁴⁵.

	$dE_g/dT _{\text{expt.}}$	dE_g/dT	$dE_g/dT _{\text{EPC}}$	EPC
	(10^{-4} eV/K)			Pct.
r-MAPbBr ₃	2.8	5.8	4.0	71%
p-FAPbBr ₃	4.9	3.6	1.2	34%
p-MAPbBr ₃	2.8	2.9	2.0	70%
p-CsPbBr ₃	3.4	2.6	2.4	94%
p-FAPbI ₃	4.3	4.6	3.2	70%
p-MAPbI ₃	2.6	3.1	2.7	88%
p-CsPbI ₃	8.5	1.2	1.2	97%
p-FASnI ₃	9.8	8.0	2.2	27%
p-MASnI ₃	4.5	5.7	3.5	61%
p-CsSnI ₃	4.8	3.9	3.3	84%

larger dE_g/dT , which we attribute to positional polymorphism enhancing band gap renormalization via TE. This effect is driven by the stronger lone pair activity⁸⁴ of Sn that promotes Sn-I-Sn bending under lattice expansion⁴⁵.

Now we analyze the effect of local disorder in the electronic structure of hybrid halide perovskites without thermal effects. In Figs. 2(a) and (b), we compare the electron spectral functions (color maps) obtained for the polymorphous cubic FAPbI₃ and MASnI₃ with the band structures (black lines) calculated for their monomorphous networks. Spectral functions were calculated using band unfolding⁸⁵ including spin orbit coupling (SOC) as implemented in `bands_unfold.x` of the EPW/ZG module^{68,69}. Local disorder leads to significant changes in the electronic structure, including enhanced band broadenings and gap openings. Particularly, our calculations for the polymorphous cubic FAPbI₃ yield an average hole and electron effective mass enhancements^{45,86} of $\lambda_h = 2.3$ and $\lambda_e = 2.0$, and a gap opening of $\Delta E_g = 0.24$ eV compared to the reference structure. The latter value compares well with $\Delta E_g = 0.29$ eV with respect to the monomorphous structure, reported in Ref. [1]. The corresponding results for polymorphous MASnI₃ are $\Delta E_g = 0.37$ eV, $\lambda_h = 1.2$, and $\lambda_e = 3.0$.

Figure 2(c) show the dependence of the band gap increase due to positional polymorphism ΔE_g in hybrid halide perovskites on the average bond angle decrease $\Delta\theta_{B-X-B}$. For completeness, we also include data for Cs- and Cl-based halide perovskites from Ref. [45]. The measure^{87,88} $\Delta\theta_{B-X-B}$ is strongly correlated with bond length changes⁴⁵ and thereby is chosen as the main descriptor for quantifying local disorder with respect to the high-symmetry inorganic network. Our calculations and analysis yield ΔE_g in the range 198–616 meV and a slope of 22 meV/(°), revealing a strong correlation between ΔE_g and bond angles change with a Pearson correlation of $r = 0.96$. This is expected, as deviations in bond angles from their ideal values lead to a reduction in

the antibonding coupling between metal and halogen orbitals^{45,88–91}. The high R^2 of 0.92 show that this distortion measure can effectively explain the gap opening due to positional polymorphism. Furthermore, the band gap variability, computed for 10 configurations and shown as error bars [Fig. 2(c)], is larger for MA-based compounds due to the larger dipole moments of the MA compared to the FA cations^{56,92}. Cl compounds, e.g. MAPbCl₃, exhibit the largest band gap variability under local disorder because the smaller, more electronegative Cl ions create stronger Pb-Cl bonds, making the band structure highly sensitive to structural distortions.

Compared to their reference structures, polymorphous cubic FA, MA, and Cs-based compounds exhibit total energy lowerings of 50–73 meV/f.u., 53–93 meV/f.u., and

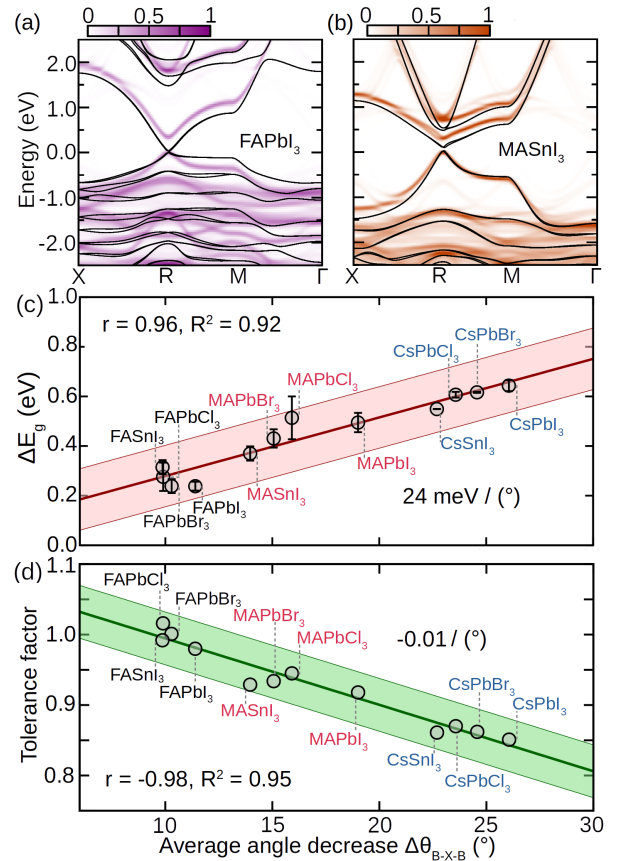


FIG. 2. (a,b) Electron spectral functions (color maps) of the polymorphous cubic FAPbI₃ (a) and MASnI₃ (b). Black dispersions represent the band structure of the monomorphous networks. (c,d) Average band gap increase due to positional polymorphism ΔE_g (c) and tolerance factor t (d) versus the average metal-halide-metal angle decrease $\Delta\theta_{B-X-B}$ calculated for 10 distinct polymorphous configurations with different starting random orientations of the molecules. Solid lines are fits obtained by linear regression and shaded regions represent three standard deviations on either side of the lines. The error bars represent the maximum absolute deviation from the average band gap evaluated for each material.

61–121 meV/f.u., respectively⁴⁵. This trend highlights the role of A-cation size in stabilizing locally disordered phases, with smaller cations facilitating structural distortions^{93,94}. This is further illustrated in Figs. 2(c) and (d), where bond angle variations depend strongly on the cations and the tolerance factors. We evaluate the tolerance factors (t) using ionic radii of 1.19, 1.15, 2.2, 1.96, 1.81, 1.88, 2.2, and 2.5 Å for Pb²⁺, Sn²⁺, I⁻, Br⁻, Cl⁻, Cs⁺, MA⁺, and FA^{+95,96}, respectively. Our analysis suggests that smaller tolerance factors allow for greater local disorder, and thus larger band gap openings. For instance, the relatively low tolerance factors of Cs-based halide perovskites ($t = 0.85$ –0.87) facilitate octahedral distortion due to the absence of larger organic A-site cations^{93,94,97}. This structural flexibility promotes a higher local disorder, which leads to significant band gap renormalizations exceeding 0.55 eV. Similarly, MA-based compounds exhibit a higher degree of polymorphism, smaller t , and larger ΔE_g than FA-based compounds, attributable to the smaller size of MA.

At this point, we emphasize that local disorder in hybrid halide perovskites appears to be a key factor in determining the band gap order between FA- and MA-based compounds. For example, as shown in Fig. 1(g), MA-based cubic lead halide perovskites have a larger band gap compared to their FA-based counter-

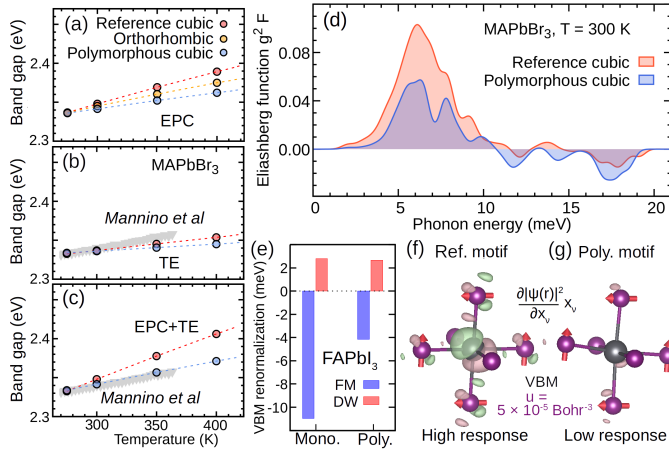


FIG. 3. (a,b,c) Temperature-dependent band gap of cubic MAPbBr₃ calculated considering (a) electron-phonon coupling (EPC), (b) lattice thermal expansion (TE), and (c) both effects combined. Calculated data are shifted by 1.38 eV (orthorhombic), 1.79 eV (monomorphous cubic) and 1.44 eV (polymorphous cubic) to match the experiment⁴⁹ (grey triangles) at $T = 275$ K. (d) Eliashberg function showing the one-phonon energy-resolved band gap renormalization of MAPbBr₃ at $T = 300$ K. (e) Fan-Migdal (FM) and Debye-Waller (DW) self-energy corrections to the VBM of the reference and polymorphous cubic FAPbI₃ due to a bending mode. (f,g) Linear variations in the charge density at the VBM obtained for a single motif of the reference (f) and polymorphous (g) networks. Arrows representing the bending mode are scaled by 50. The isosurface value u is indicated.

parts within the same temperature range. The difference can be attributed to the band gap widenings reported in Fig. 2(c). In the case of tin halide perovskites, the situation is reversed, a trend that agrees with experiments, as shown in Fig. 1(h). This observation is explained, e.g., by the larger TE coefficient of FASnI₃⁷⁷, together with the greater propensity for lone pair expression in sterically constrained FA-based compounds, which enhance thermal-induced band gap renormalization.

We next elucidate the mechanisms determining the band gap temperature coefficient of halide perovskites. Figure 3(a) shows the electron-phonon renormalized band gap of MAPbBr₃ as a function of temperature calculated for the ZG reference (red) and ZG polymorphous (blue) cubic structures, both generated using stable anharmonic phonons. Local disorder significantly affects EPC, leading to a slower band gap variation with temperature. On the same plot, we include calculations for the orthorhombic structure (orange) using harmonic phonons. Attempting to mimic positional polymorphism at high temperatures using the orthorhombic phase does not accurately capture the effect of EPC. Notably, polymorphism also affects the band gap widening due to TE, as shown in Fig. 3(b); a point that has been overlooked in previous calculations^{36,82,98,99}. Accounting for local disorder in our calculations reduces the band gap opening due to TE by 50% and the slope $dE_g/dT|_{\text{TE}}$ alone underestimates significantly the experimental data⁴⁹.

In Fig. 3(c), we show that combining EPC and lattice expansion in our calculations for the polymorphous cubic MAPbBr₃, the total dE_g/dT yields excellent agreement with experiment. In contrast, dE_g/dT is overestimated by a factor of two when the ZG reference network is used. A quantitative comparison of dE_g/dT alongside the percentage contribution of EPC for reference and polymorphous MAPbBr₃ is presented in Table I.

Figure 3(d) shows the one-phonon energy-resolved contribution to the band gap renormalization of MAPbBr₃ at $T = 300$ K calculated using the Eliashberg function: $g^2 F_n(\omega, T) = \sum_{\nu} \Delta \varepsilon_{n,\nu}(T) \delta(\hbar\omega - \hbar\omega_{\nu})$. Here, $\hbar\omega_{\nu}$ is the phonon energy of mode ν , $\Delta \varepsilon_{n,\nu}(T) = \frac{1}{2} \frac{\partial^2 \varepsilon_n}{\partial x_{\nu}^2} \sigma_{\nu,T}^2$ is the mode-resolved energy renormalization of a state ψ_n up to second order, and $\sigma_{\nu,T}^2$ is the associated mean-square displacement¹⁰⁰. $\Delta \varepsilon_{n,\nu}(T)$ is calculated by finite differences using single mode displaced configurations generated by ZG.x⁶⁹. Our results for the reference and polymorphous structures reveal that low energy optical vibrations in the window 2–10 meV and 4–10 meV, respectively, dominate the phonon-induced band gap widening, in agreement with interpretations of previous works^{6,23,101,102}. The modes associated with this energy window have a bending or rocking character, associated with variations in the B-X-B bond angles and octahedral tilting¹⁰³. Higher frequency modes are mostly associated to B-X stretching or molecular librations. Positional polymorphism strongly suppresses the positive EPC contribution in the window 2–10 meV, while enhancing the negative contributions in the window 10–20 meV, resulting in significant reduction

in the overall gap opening.

To elucidate the origin of this reduction, we investigate the band gap renormalization due to a mode with bending character. If we consider the Kohn-Sham hamiltonian H_{KS} , express $\varepsilon_n = \langle \psi_n | H_{\text{KS}} | \psi_n \rangle$, take the second derivative with x_ν , and apply the Hellmann-Feynman theorem twice¹⁰⁴ we obtain:

$$\frac{\partial^2 \varepsilon_n}{\partial x_\nu^2} = \int d\mathbf{r} \frac{\partial V_{\text{KS}}}{\partial x_\nu} \frac{\partial |\psi_n(\mathbf{r})|^2}{\partial x_\nu} + \int d\mathbf{r} \frac{\partial^2 V_{\text{KS}}}{\partial x_\nu^2} |\psi_n(\mathbf{r})|^2. \quad (2)$$

Here, V_{KS} is the Kohn-Sham potential and the integration is taken over all electron coordinates \mathbf{r} . To arrive at this expression we also neglected the non-local contribution to V_{KS} ¹⁰⁵. The first and second terms on the right hand side of Eq. (2) are the Fan-Migdal (FM) and Debye-Waller (DW) EPC coefficients⁸⁶.

Figure 3(e) shows the FM and DW self-energy corrections to the valence band maximum (VBM) induced by nuclei vibrations of amplitude 0.02 Å along a bending mode. We present results for the reference and polymorphous networks of FAPbI₃. In both cases, the negative FM dominates over the positive DW correction leading to an overall energy decrease of the VBM of 8.2 meV and 1.5 meV for the reference and polymorphous networks, respectively. This contributes to the band gap opening in both cases. The relatively large difference in the VBM energy decrease is associated to the strong reduction of the FM term (62%) when we employ a polymorphous network. This result can be explained by inspecting the changes of the electronic charge distribution at the VBM in response to the movement of the nuclei along the bending mode (i.e. $\partial |\psi(\mathbf{r})|^2 / \partial x_\nu$), shown in Figs. 3(f) and (g). The charge density in the reference structure exhibits a higher response to the nuclear vibrations than that in the polymorphous structure, leading essentially to a much larger self-energy correction. The reduced response in the polymorphous structure arises from the deviation of Pb-I-Pb bond angles from 180°, which disrupts orbital overlap and localizes the electronic states, thereby weakening the electron-phonon coupling. On the other hand, the DW corrections to the VBM of the reference and polymorphous structures are nearly the same [Fig. 3(e)], as the charge density $|\psi(\mathbf{r})|^2$ remains the same and concentrated around the I atoms. A similar behavior is observed for the conduction band minimum (CBM), where the DW terms remain similar while the positive FM term, leading to a CBM energy increase, is reduced by 71% due to local disorder.

In conclusion, we demonstrate an efficient method for the calculation of temperature-dependent band gaps in

complex polymorphous systems based on the ASDM. Our method allows for the simultaneous treatment of anharmonicity and local disorder in both the inorganic and organic sublattices, as well as electron-phonon coupling. We clarify the origin of the gradual band gap blueshift of halide perovskites with temperature, attributing it to the low response of electrons to nuclear vibrations induced by positional polymorphism. Our bottom-up *ab initio* approach allows for disentangling effects of local disorder, electron-phonon coupling, and thermal expansion, enabling our understanding of the individual role of these key phenomena in optoelectronic properties. In addition, we elucidate the key role of the A-site cation in influencing local disorder, band gap, and the electron-phonon renormalization. In the future, it will be interesting to investigate temperature-dependent properties of layered halide perovskites and heterostructures^{29,30,106}. Our approach also forms the basis for anharmonic electron-phonon calculations in polymorphous solids, including the study of phonon-assisted optical absorption^{100,107,108}, carrier mobilities^{39,109–111}, polarons^{102,112–116}, and exciton-phonon interactions^{117,118}.

ACKNOWLEDGMENTS

This research was funded by the European Union (project ULTRA-2DPK / HORIZON-MSCA-2022-PF-01 / Grant Agreement No. 101106654). Views and opinions expressed are however those of the authors only and do not necessarily reflect those of the European Union or the European Commission. Neither the European Union nor the granting authority can be held responsible for them. We thank D. R. Ceratti for graciously providing data on temperature-dependent band gaps of Br-based hybrid halide perovskite single crystals. J.E. acknowledges financial support from the Institut Universitaire de France. F.G. was supported by the the Robert A. Welch Foundation under Award No. F-2139-20230405 and by the National Science Foundation under DMREF Grant No. 2119555. G.V. acknowledges funding from the ANR through the CPJ program and the SURFIN project (ANR-23-CE09-0001), the ALSATIAN project (ANR-23-CE50-0030), and the ANR under the France 2030 programme, MINOTAURE project (ANR-22-PETA-0015). We acknowledge that the results of this research have been achieved using computational resources from the EuroHPC Joint Undertaking and supercomputer LUMI [<https://lumi-supercomputer.eu/>], hosted by CSC (Finland) and the LUMI consortium through a EuroHPC Extreme Scale Access call.

* zachariasmarios@gmail.com

† jacky.even@insa-rennes.fr

¹ X.-G. Zhao, G. M. Dalpian, Z. Wang, and A. Zunger, Phys. Rev. B **101**, 155137 (2020).

- ² Z. Wang, X.-G. Zhao, R. Koch, S. J. L. Billinge, and A. Zunger, Phys. Rev. B **102**, 235121 (2020).
- ³ D. H. Fabini, R. Seshadri, and M. G. Kanatzidis, MRS Bull. **45**, 467–477 (2020).
- ⁴ Z. Wang, O. I. Malyi, X. Zhao, and A. Zunger, Phys. Rev. B **103**, 165110 (2021).
- ⁵ M. G. Goesten, Y. Xia, U. Aschauer, and M. Amsler, J. Am. Chem. Soc. **144**, 3398 (2022).
- ⁶ M. Zacharias, G. Volonakis, F. Giustino, and J. Even, npj Comput. Mater. **9**, 153 (2023).
- ⁷ D. N. Dirin, A. Vivani, M. Zacharias, T. V. Sekh, I. Cherniukh, S. Yakunin, F. Bertolotti, M. Aebl, R. D. Schaller, A. Wieczorek, *et al.*, Nano Lett. **23**, 1914 (2023).
- ⁸ S. Sabisch, M. Aebl, A. Kanak, V. Morad, S. C. Boehme, M. Wörle, L. G. Feld, C. Copéret, and M. V. Kovalenko, Chem. Mater. (2025).
- ⁹ Y. Wang, M. Zacharias, X. Zhang, N. Pant, J. Even, P. F. P. Poudeu, and E. Kioupakis, “Efficient first-principles framework for overdamped phonon dynamics and anharmonic electron-phonon coupling in superionic materials,” (2025), arXiv:2502.07217.
- ¹⁰ R. Comes, M. Lambert, and A. Guinier, Solid State Commun. **6**, 715 (1968).
- ¹¹ K. Itoh, K. Ochiai, H. Kawaguchi, C. Moriyoshi, and E. Nakamura, Ferroelectrics **159**, 85 (1994).
- ¹² H. Mashiyama, Y. Kurihara, and T. Azestu, J. Korean Phys. Soc. **32**, S156 (1998).
- ¹³ J.-M. Kiat, G. Baldinozzi, M. Dunlop, C. Malibert, B. Dkhil, C. Ménoret, O. Masson, and M.-T. Fernandez-Diaz, J. Phys. Condens. Matter. **12**, 8411–8425 (2000).
- ¹⁴ R. J. Worhatch, H. Kim, I. P. Swainson, A. L. Yonkeu, and S. J. L. Billinge, Chem. Mater. **20**, 1272 (2008).
- ¹⁵ A. N. Beecher, O. E. Semonin, J. M. Skelton, J. M. Frost, M. W. Terban, H. Zhai, A. Alatas, J. S. Owen, A. Walsh, and S. J. L. Billinge, ACS Energy Lett. **1**, 880 (2016).
- ¹⁶ M. S. Senn, D. A. Keen, T. C. A. Lucas, J. A. Hriljac, and A. L. Goodwin, Phys. Rev. Lett. **116**, 207602 (2016).
- ¹⁷ G. Laurita, D. H. Fabini, C. C. Stoumpos, M. G. Kanatzidis, and R. Seshadri, Chem. Sci. **8**, 5628–5635 (2017).
- ¹⁸ R. J. Sutton, M. R. Filip, A. A. Haghvirad, N. Sakai, B. Wenger, F. Giustino, and H. J. Snaith, ACS Energy Lett. **3**, 1787 (2018).
- ¹⁹ A. C. Ferreira, S. Paofai, A. Létoublon, J. Ollivier, S. Raymond, B. Hehlen, B. Rufflé, S. Cordier, C. Katan, J. Even, and P. Bourges, Commun. Phys. **3**, 48 (2020).
- ²⁰ T. A. S. Doherty, S. Nagane, D. J. Kubicki, Y.-K. Jung, D. N. Johnstone, A. N. Iqbal, D. Guo, K. Frohma, M. Danaie, E. M. Tennyson, *et al.*, Science **374**, 1598 (2021).
- ²¹ M. Morana, J. Wiktor, M. Coduri, R. Chiara, C. Giacobbe, E. L. Bright, F. Ambrosio, F. D. Angelis, and L. Malavasi, J. Phys. Chem. Lett. **14**, 2178 (2023).
- ²² N. J. Wedock, C. MacKeen, X. Qin, L. Waquier, Y. Rakita, J. A. Vigil, H. I. Karunadasa, V. Blum, M. F. Toney, and F. Bridges, PRX Energy **2**, 033004 (2023).
- ²³ N. Yazdani, M. I. Bodnarchuk, F. Bertolotti, N. Masicocchi, I. Furera, B. GuzelTurk, B. L. Cotts, M. Zajac, G. Rainò, M. Jansen, *et al.*, Nat. Phys. , 47–53 (2023).
- ²⁴ X. He, M. Krogstad, M. K. Gupta, T. Lanigan-Atkins, C. Mao, F. Ye, Y. Liu, T. Hong, S. Chi, H. Wei, J. Huang, *et al.*, PRX Energy **3**, 013014 (2024).
- ²⁵ M. Dubajic, J. R. Neilson, J. Klarbring, X. Liang, S. A. Bird, K. C. Rule, J. E. Auckett, T. A. Selby, G. Tumen-Ulzii, Y. Lu, *et al.*, Nat. Nanotechnol. (2025).
- ²⁶ A. Kojima, K. Teshima, Y. Shirai, and T. Miyasaka, J. Am. Chem. Soc. **131**, 6050 (2009).
- ²⁷ H. J. Snaith, J. Phys. Chem. Lett. **4**, 3623–3630 (2013).
- ²⁸ K. Lin, J. Xing, L. N. Quan, F. P. G. de Arquer, X. Gong, J. Lu, L. Xie, W. Zhao, D. Zhang, C. Yan, *et al.*, Nature **562**, 245–248 (2018).
- ²⁹ S. Sidhik, Y. Wang, M. De Siena, R. Asadpour, A. J. Torma, T. Terlier, K. Ho, W. Li, A. B. Puthirath, X. Shuai, *et al.*, Science **377**, 1425–1430 (2022).
- ³⁰ I. Metcalf, S. Sidhik, H. Zhang, A. Agrawal, J. Persaud, J. Hou, J. Even, and A. D. Mohite, Chem. Rev. **123**, 9565 (2023).
- ³¹ J.-P. Correa-Baena, M. Saliba, T. Buonassisi, M. Grätzel, A. Abate, W. Tress, and A. Hagfeldt, Science **358**, 739 (2017).
- ³² L. Mao, W. Ke, L. Pedesseau, Y. Wu, C. Katan, J. Even, M. R. Wasielewski, C. C. Stoumpos, and M. G. Kanatzidis, J. Am. Chem. Soc. **140**, 3775–3783 (2018).
- ³³ J. Even, L. Pedesseau, J.-M. Jancu, and C. Katan, J. Phys. Chem. Lett. **4**, 2999 (2013).
- ³⁴ J. Even, L. Pedesseau, J.-M. Jancu, and C. Katan, physica status solidi (RRL) – Rapid Research Letters **8**, 31 (2013).
- ³⁵ A. Amat, E. Mosconi, E. Ronca, C. Quart, P. Umari, M. K. Nazeeruddin, M. Grätzel, and F. D. Angelis, Nano Lett. **14**, 3608 (2014).
- ³⁶ W. A. Saidi, S. Poncé, and B. Monserrat, J. Phys. Chem. Lett. **7**, 5247 (2016).
- ³⁷ L. D. Whalley, J. M. Frost, Y.-K. Jung, and A. Walsh, J. Chem. Phys. **146**, 220901 (2017).
- ³⁸ B. Traoré, G. Bouder, W. Lafargue-Dit-Hauret, X. Rocquefelte, C. Katan, F. Tran, and M. Kepenekian, Phys. Rev. B **99**, 035139 (2019).
- ³⁹ S. Poncé, M. Schlipf, and F. Giustino, ACS Energy Lett. **4**, 456 (2019).
- ⁴⁰ H. M. Ghaitan, Z. A. Alahmed, S. M. H. Qaid, M. Hezam, and A. S. Aldwayyan, ACS Omega **5**, 7468 (2020).
- ⁴¹ M. Zacharias, G. Volonakis, F. Giustino, and J. Even, Phys. Rev. B **108**, 035155 (2023).
- ⁴² C. Katan, A. D. Mohite, and J. Even, Nat. Mater. **17**, 377 (2018).
- ⁴³ C. Quart, R. Gautier, M. Zacharias, A. Gansmuller, and C. Katan, J. Am. Chem. Soc. **147**, 278–291 (2024).
- ⁴⁴ I. B. Garba, L. Trombini, C. Katan, J. Even, M. Zacharias, M. Kepenekian, and G. Volonakis, ACS Mater. Lett. **7**, 1922–1929 (2025).
- ⁴⁵ M. Zacharias, G. Volonakis, L. Pedesseau, C. Katan, F. Giustino, and J. Even, Companion Long Paper (2025).
- ⁴⁶ R. L. Milot, G. E. Eperon, H. J. Snaith, M. B. Johnston, and L. M. Herz, Adv. Funct. Mater. **25**, 6218–6227 (2015).
- ⁴⁷ A. G. Kontos, A. Kaltzoglou, M. K. Arfanis, K. M. McCall, C. C. Stoumpos, B. W. Wessels, P. Falaras, and M. G. Kanatzidis, J. Phys. Chem. C **122**, 26353–26361 (2018).
- ⁴⁸ E. S. Parrott, R. L. Milot, T. Stergiopoulos, H. J. Snaith, M. B. Johnston, and L. M. Herz, J. Phys. Chem. Lett. **7**, 1321–1326 (2016).
- ⁴⁹ G. Mannino, I. Deretis, E. Smecca, A. La Magna, A. Alberti, D. Ceratti, and D. Cahen, J. Phys. Chem. Lett. **11**, 2490–2496 (2020).
- ⁵⁰ Y. Chen, Y. Lei, Y. Li, Y. Yu, J. Cai, M.-H. Chiu, R. Rao, Y. Gu, C. Wang, W. Choi, *et al.*, Nature **577**, 209–215

- (2020).
- ⁵¹ S. Kahmann, O. Nazarenko, S. Shao, O. Hordiichuk, M. Kepenekian, J. Even, M. V. Kovalenko, G. R. Blake, and M. A. Loi, *ACS Energy Lett.* **5**, 2512 (2020).
- ⁵² C. Quarti, E. Mosconi, and F. De Angelis, *Phys. Chem. Chem. Phys.* **17**, 9394–9409 (2015).
- ⁵³ C. Quarti, E. Mosconi, J. M. Ball, V. D’Innocenzo, C. Tao, S. Pathak, H. J. Snaith, A. Petrozza, and F. D. Angelis, *Energy Environ. Sci.* **9**, 155 (2016).
- ⁵⁴ J. Even, M. Carignano, and C. Katan, *Nanoscale* **8**, 6222 (2016).
- ⁵⁵ J. Wiktor, U. Rothlisberger, and A. Pasquarello, *J. Phys. Chem. Lett.* **8**, 5507 (2017).
- ⁵⁶ M. A. Carignano, S. A. Aravindh, I. S. Roqan, J. Even, and C. Katan, *J. Phys. Chem. C* **121**, 20729–20738 (2017).
- ⁵⁷ J. Lahnsteiner and M. Bokdam, *Phys. Rev. B* **105**, 024302 (2022).
- ⁵⁸ V. Diez-Cabanes, S. Giannini, D. Beljonne, and C. Quarti, *Adv. Opt. Mater.* **12**, 2301105 (2023).
- ⁵⁹ S. A. Seidl, X. Zhu, G. Reuveni, S. Aharon, C. Gehrmann, S. Caicedo-Dávila, O. Yaffe, and D. A. Egger, *Phys. Rev. Mater.* **7**, L092401 (2023).
- ⁶⁰ D. Dai, S. Agrawal, O. V. Prezhdo, and R. Long, *J. Chem. Phys.* **160** (2024), 10.1063/5.0202251.
- ⁶¹ P. Giannozzi *et al.*, *J. Phys.: Condens. Matter* **21**, 395502 (2009).
- ⁶² P. Giannozzi *et al.*, *J. Phys.: Condens. Matter* **29**, 465901 (2017).
- ⁶³ D. R. Hamann, *Phys. Rev. B* **88**, 085117 (2013).
- ⁶⁴ M. van Setten, M. Giantomassi, E. Bousquet, M. Verstraete, D. Hamann, X. Gonze, and G.-M. Rignanese, *Comput. Phys. Commun.* **226**, 39 (2018).
- ⁶⁵ J. P. Perdew, A. Ruzsinszky, G. I. Csonka, O. A. Vydrov, G. E. Scuseria, L. A. Constantin, X. Zhou, and K. Burke, *Phys. Rev. Lett.* **100**, 136406 (2008).
- ⁶⁶ C. Motta, F. El-Mellouhi, S. Kais, N. Tabet, F. Alharbi, and S. Sanvito, *Nat. Commun.* **6**, 7026 (2015).
- ⁶⁷ C. E. P. Villegas, A. R. Rocha, and A. Marini, *Nano Lett.* **16**, 5095–5101 (2016).
- ⁶⁸ M. Zacharias and F. Giustino, *Phys. Rev. Res.* **2**, 013357 (2020).
- ⁶⁹ H. Lee, S. Poncé, K. Bushick, S. Hajinazar, J. Lafuente-Bartolome, J. Leveillée, C. Lian, J.-M. Lihm, F. Macheda, H. Mori, *et al.*, *npj Comput. Mater.* **9**, 156 (2023).
- ⁷⁰ Y. Kawamura, H. Mashiyama, and K. Hasebe, *Journal of the Physical Society of Japan* **71**, 1694–1697 (2002).
- ⁷¹ H. Mashiyama, Y. Kawamura, E. Magome, and Y. Kubota, *J. Korean Phys. Soc.* **42**, 1026 (2003).
- ⁷² C. C. Stoumpos, C. D. Malliakas, J. A. Peters, Z. Liu, M. Sebastian, J. Im, T. C. Chasapis, A. C. Wibowo, D. Y. Chung, A. J. Freeman, B. W. Wessels, and M. G. Kanatzidis, *Cryst. Growth Des.* **13**, 2722–2727 (2013).
- ⁷³ Y. Rakita, S. R. Cohen, N. K. Kedem, G. Hodes, and D. Cahen, *MRS Commun.* **5**, 623–629 (2015).
- ⁷⁴ P. S. Whitfield, N. Herron, W. E. Guise, K. Page, Y. Q. Cheng, I. Milas, and M. K. Crawford, *Sci. Rep.* **6**, 35685 (2016).
- ⁷⁵ Y. Dang, Y. Zhou, X. Liu, D. Ju, S. Xia, H. Xia, and X. Tao, *Angew. Chem. Int. Ed.* **55**, 3447–3450 (2016).
- ⁷⁶ D. H. Fabini, C. C. Stoumpos, G. Laurita, A. Kaltzoglou, A. G. Kontos, P. Falaras, M. G. Kanatzidis, and R. Seshadri, *Angew. Chem. Int. Ed.* **55**, 15392–15396 (2016).
- ⁷⁷ E. C. Schueller, G. Laurita, D. H. Fabini, C. C. Stoumpos, M. G. Kanatzidis, and R. Seshadri, *Inorg. Chem.* **57**, 695–701 (2017).
- ⁷⁸ A. Marronnier, G. Roma, S. Boyer-Richard, L. Pedesseau, J.-M. Jancu, Y. Bonnassieux, C. Katan, C. C. Stoumpos, M. G. Kanatzidis, and J. Even, *ACS Nano* **12**, 3477–3486 (2018).
- ⁷⁹ M. Keshavarz, M. Ottesen, S. Wiedmann, M. Wharmby, R. Küchler, H. Yuan, E. Debroye, J. A. Steele, J. Martens, N. E. Hussey, *et al.*, *Adv. Mater.* **31**, 1900521 (2019).
- ⁸⁰ T. Handa, H. Tahara, T. Aharen, A. Shimazaki, A. Wakamiya, and Y. Kanemitsu, *Phys. Rev. Mater.* **4**, 074604 (2020).
- ⁸¹ Y. He, C. C. Stoumpos, I. Hadar, Z. Luo, K. M. McCall, Z. Liu, D. Y. Chung, B. W. Wessels, and M. G. Kanatzidis, *J. Am. Chem. Soc.* **143**, 2068–2077 (2021).
- ⁸² A. Francisco-López, B. Charles, O. J. Weber, M. I. Alonso, M. Garriga, M. Campoy-Quiles, M. T. Weller, and A. R. Goñi, *J. Phys. Chem. Lett.* **10**, 2971–2977 (2019).
- ⁸³ A. Rubino, A. Francisco-López, A. J. Barker, A. Petrozza, M. E. Calvo, A. R. Goñi, and H. Míguez, *J. Phys. Chem. Lett.* **12**, 569–575 (2020).
- ⁸⁴ A. Balvanz, M. Safdari, M. Zacharias, D. Kim, C. Welton, E. H. Oriel, M. Kepenekian, C. Katan, C. D. Malliakas, J. Even, V. Klepov, G. N. Manjunatha Reddy, R. D. Schaller, L. X. Chen, R. Seshadri, and M. G. Kanatzidis, *J. Am. Chem. Soc.* **146**, 16128–16147 (2024).
- ⁸⁵ V. Popescu and A. Zunger, *Phys. Rev. B* **85**, 085201 (2012).
- ⁸⁶ F. Giustino, *Rev. Mod. Phys.* **89**, 015003 (2017).
- ⁸⁷ W. H. Baur, *Acta Crystallographica Section B Structural Crystallography and Crystal Chemistry* **30**, 1195–1215 (1974).
- ⁸⁸ M. R. Filip, G. E. Eperon, H. J. Snaith, and F. Giustino, *Nat. Commun.* **5**, 5757 (2014).
- ⁸⁹ J. L. Knutson, J. D. Martin, and D. B. Mitzi, *Inorg. Chem.* **44**, 4699–4705 (2005).
- ⁹⁰ M. I. Dar, G. Jacopin, S. Meloni, A. Mattoni, N. Arora, A. Bozik, S. M. Zakeeruddin, U. Rothlisberger, and M. Grätzel, *Sci. Adv.* **2** (2016), 10.1126/sciadv.1601156.
- ⁹¹ S. Meloni, G. Palermo, N. Ashari-Astani, M. Grätzel, and U. Rothlisberger, *J. Chem. Mater. A* **4**, 15997–16002 (2016).
- ⁹² S. Maheshwari, M. B. Fridriksson, S. Seal, J. Meyer, and F. C. Grozema, *J. Phys. Chem. C* **123**, 14652–14661 (2019).
- ⁹³ G. Kieslich, S. Sun, and A. K. Cheetham, *Chem. Sci.* **5**, 4712–4715 (2014).
- ⁹⁴ X. Li, M. Kepenekian, L. Li, H. Dong, C. C. Stoumpos, R. Seshadri, C. Katan, P. Guo, J. Even, and M. G. Kanatzidis, *J. Am. Chem. Soc.* **144**, 3902–3912 (2022).
- ⁹⁵ R. D. Shannon, *Acta Crystallographica Section A* **32**, 751–767 (1976).
- ⁹⁶ G. Kieslich, S. Sun, and A. K. Cheetham, *Chem. Sci.* **6**, 3430–3433 (2015).
- ⁹⁷ M. R. Filip and F. Giustino, *Proc. Natl. Acad. Sci.* **115**, 5397–5402 (2018).
- ⁹⁸ B. J. Foley, D. L. Marlowe, K. Sun, W. A. Saidi, L. Scudiero, M. C. Gupta, and J. J. Choi, *Appl. Phys. Lett.* **106**, 243904 (2015).
- ⁹⁹ J. Ning, L. Zheng, W. Lei, S. Wang, J. Xi, and J. Yang, *Phys. Chem. Chem. Phys.* **24**, 16003–16010 (2022).

- ¹⁰⁰ M. Zacharias and F. Giustino, Phys. Rev. B **94**, 075125 (2016).
- ¹⁰¹ C. Zhu, L. G. Feld, M. Svyrydenko, I. Cherniukh, D. N. Dirin, M. I. Bodnarchuk, V. Wood, N. Yazdani, S. C. Boehme, M. V. Kovalenko, and G. Rainò, Adv. Opt. Mater. **12** (2024), 10.1002/adom.202301534.
- ¹⁰² S. Biswas, R. Zhao, F. Alowa, M. Zacharias, S. Sharifzadeh, D. F. Coker, D. S. Seferos, and G. D. Scholes, Nat. Mater. **23**, 937–943 (2024).
- ¹⁰³ M. A. Pérez-Osorio, R. L. Milot, M. R. Filip, J. B. Patel, L. M. Herz, M. B. Johnston, and F. Giustino, J. Phys. Chem. C **119**, 25703–25718 (2015).
- ¹⁰⁴ S. Poncé, G. Antonius, Y. Gillet, P. Boulanger, J. Laflamme Janssen, A. Marini, M. Côté, and X. Gonze, Phys. Rev. B **90**, 214304 (2014).
- ¹⁰⁵ A. F. Starace, Phys. Rev. A **3**, 1242 (1971).
- ¹⁰⁶ J. Jiang, T. van der Heide, S. Thébaud, C. R. Lien-Medrano, A. Fihey, L. Pedesseau, C. Quarti, M. Zacharias, G. Volonakis, M. Kepenekian, *et al.*, Phys. Rev. Mater. **9**, 023803 (2025).
- ¹⁰⁷ M. Zacharias, C. E. Patrick, and F. Giustino, Phys. Rev. Lett. **115**, 177401 (2015).
- ¹⁰⁸ J. Noffsinger, E. Kioupakis, C. G. Van de Walle, S. G. Louie, and M. L. Cohen, Phys. Rev. Lett. **108**, 167402 (2012).
- ¹⁰⁹ L. M. Herz, ACS Energy Lett. **2**, 1539–1548 (2017).
- ¹¹⁰ M. Schlipf, S. Poncé, and F. Giustino, Phys. Rev. Lett. **121**, 086402 (2018).
- ¹¹¹ B. Cucco, J. Leveillee, V.-A. Ha, J. Even, M. Kepenekian, F. Giustino, and G. Volonakis, PRX Energy **3**, 023012 (2024).
- ¹¹² C. Franchini, M. Reticcioli, M. Setvin, and U. Diebold, Nat. Rev. Mater. **6**, 560–586 (2021).
- ¹¹³ L. P. René de Cotret, M. R. Otto, J.-H. Pöhls, Z. Luo, M. G. Kanatzidis, and B. J. Siwick, Proc. Natl. Acad. Sci. **119**, e2113967119 (2022).
- ¹¹⁴ J. Lafuente-Bartolome, C. Lian, W. H. Sio, I. G. Gurtubay, A. Eiguren, and F. Giustino, Phys. Rev. Lett. **129**, 076402 (2022).
- ¹¹⁵ H. Zhang, W. Li, J. Essman, C. Quarti, I. Metcalf, W.-Y. Chiang, S. Sidhik, J. Hou, A. Fehr, A. Attar, *et al.*, Nat. Phys. **19**, 545–550 (2023).
- ¹¹⁶ H. Seiler, D. Zahn, V. C. A. Taylor, M. I. Bodnarchuk, Y. W. Windsor, M. V. Kovalenko, and R. Ernstorfer, ACS Nano **17**, 1979–1988 (2023).
- ¹¹⁷ A. M. Alvertis, J. B. Haber, E. A. Engel, S. Sharifzadeh, and J. B. Neaton, Phys. Rev. Lett. **130**, 086401 (2023).
- ¹¹⁸ Z. Dai, C. Lian, J. Lafuente-Bartolome, and F. Giustino, Phys. Rev. Lett. **132**, 036902 (2024).